The Fluid Dynamic and Shear Environment in the NASA/JSC Rotating-Wall Perfused-Vessel Bioreactor

Cynthia M. Begley, Stanley J. Kleis

[1]*United Space Alliance, L. B. Johnson Space Center, Houston, Texas, USA*
[2]*Department of Mechanical Engineering, University of Houston, Houston, Texas 77204-4792, USA; telephone: 713-743-4536; fax: 713-743-4503; e-mail: kleis@uh.edu*

Received 22 August 1999; accepted 30 March 2000

Abstract: The rotating-wall perfused-vessel (RWPV) bioreactor, used for both microgravity and Earth-based cell science experiments, is characterized in terms of the fluid dynamic and fluid shear stress environment. A numerical model of the flow field is developed and verified with laser Doppler velocimeter measurements. The effects of changes in operating conditions, including rotation rates and fluid perfusion rates, are investigated with the numerical model. The operating conditions typically used for ground-based experiments (equal rotation of the inner and outer cylinders) leads to flow patterns with relatively poor mass distribution characteristics. Approximately 50% of the inlet-perfused fluid bypasses the bulk of the fluid volume and flows to the perfusion exit. For operating conditions typical in microgravity, small differential rotation rates between the inner and outer cylinders lead to greatly improved flow distribution patterns and very low fluid shear stress levels over a large percentage of the fluid volume. Differences in flow patterns for the different operating conditions are explored. Large differences in the hydrodynamic environments for operating conditions typical of true microgravity and ground-based "microgravity simulations" are demonstrated. *Biotechnol Bioeng* **70**: 32–40, 2000.
Keywords: bioreactor design; microgravity culture; low shear culture; rotating-wall vessel; microcarrier

INTRODUCTION

The viscous pump (VP) bioreactor was developed at the University of Houston (Kleis et al., 1990) and adopted by NASA/JSC as the rotating-wall perfused-vessel (RWPV) design for the Bioreactor Development System (BDS). Flight experiments were conducted in the RWPV on the Space Shuttle missions STS-70 and STS-85 and aboard the Russian Space Station, MIR.

The RWPV was designed specifically to allow the culture of shear-sensitive mammalian cells in a microgravity environment. The culture times vary from several days on STS missions to several months for the MIR. Thus, the BDS provides capabilities for replenishing fresh medium, as well as monitoring and control of oxygen, pH, and temperature through the use of a recirculating (perfusion) flow loop.

The cells of interest are anchorage-dependent mammalian cells that have thin cell membranes. To provide the necessary attachment surface with a large surface area:volume ratio, small "microcarrier" beads (~200 mm in diameter) are suspended in fluid medium (van Wezel, 1973). Cells inoculated into the fluid medium attach to the microcarriers. After several divisions, cells can form a confluent monolayer, with 100 to 200 cells on each microcarrier. Many cell-covered microcarriers attach and bridge to form larger cell assemblages. Cell assemblages have been grown up to several millimeters in diameter (Goodwin et al., 1992).

Design Requirements

The design requirements for the vessel to be used in space are similar to those of ground-based bioreactors, with a few exceptions. For the mammalian cells of interest, mechanical shear stress levels in the range 3 to 10 dyne/cm^2 cause damage to cells and reduce cell viability (Cherry and Papoutsakis, 1986). At shear levels as low as 0.92 dyne/cm^2, cell proliferation, morphology, and function are adversely affected (Goodwin et al., 1993). Thus, to encourage three-dimensional growth and differentiation, and to further study the effects of shear on these cells, shear levels of 10^{-2} dyne/cm^2 are desired. To meet this requirement, the flow field must be laminar.

In the microgravity environment, the shapes of gas/liquid interfaces are dictated by surface tension. Gas bubbles form rather than the horizontal free surfaces commonly used for gas exchange in bioreactors operated in Earth's gravity. This, along with the concern of large stresses during dynamic coalescence of bubbles, leads to a zero-headspace (no gas phase) requirement for the bioreactor.

As with all bioreactor designs, the bioreactor system must provide a proper biological environment for the cells. For a perfused system, the vessel must provide adequate distribution of inlet fluid throughout the vessel. This requirement in the RWPV is even more stringent. To perform meaningful cell science experiments, the goal is to provide a nearly

Correspondence to: S. J. Kleis

spatially uniform environment, with adequate mass transport. That is, the fluid in the vessel should be well mixed, with a mixing time that is short compared with the time scale of the cell responses. All cells should experience nearly the same environment so that responses to particular environments can be isolated.

The cells on microcarriers and cell assemblages must be suspended in the fluid medium. Interactions with solid walls result in large shear and normal stresses and should be minimized. Settling or centrifuging of cells onto walls results in poor mass transport and/or high stress levels. Unfortunately, the operating conditions for suspension in unit gravity and microgravity are quite different and result in differences in hydrodynamic environment between cell science experiments in space and ground control experiments on Earth.

Motivation

Rotating-wall vessels (RWVs) are widely used to culture mammalian cells on Earth with the intent of simulating the microgravity environment. This and subsequent studies will show the differences between the actual microgravity cell culture environment and that of the ground-based control experiments. This first investigation will concentrate on the flow field and shear environments under a range of typical operating conditions used for both space and Earth applications. Because the hydrodynamic environments in RWVs, including the RWPV, are similar, the present results are also representative of microgravity simulations in other RWVs.

RWPV Features

The RWPV, based on the VP design, has successfully cultured mammalian cells both on Earth and in microgravity. The vessel has a concentric cylinder arrangement (see Fig. 1), with a length of 7 cm, an outer diameter of 5.0 cm, and inner cylinder diameter of 1.5 cm. The inner cylinder is porous, with a filter material covering the exit holes for extracting fluid into the external perfusion flow loop. There is a disk attached to one end of the inner cylinder (the viscous pump), which rotates with the inner cylinder. Both the inner and outer cylinders can be independently rotated. The inlet for the fluid from the external perfusion flow loop is located between the disk and vessel end cap, providing a means of keeping cells on microcarriers from entering the narrow (high shear) region behind the disk.

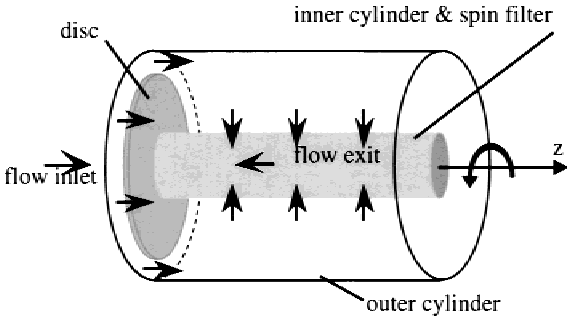

Figure 1. Rotating-wall perfused-vessel geometry.

When operated on Earth, the solid-body rotation mode is used where the inner cylinder, disk, and outer cylinder are all rotated at the same rate, between 15 and 35 rpm. As the cells grow and form aggregates, the rotation rate is increased in order to maintain off-bottom suspension as the cells fall through the fluid under the influence of gravity. For most cell types, these rotation rates are high enough to keep cells moving in circular orbits about the spin filter. For larger, more-dense cell cultures (Freed et al., 1997) a hover mode is used in which the rotation rate is just high enough to keep cell structures suspended in a stationary location.

In microgravity, rotation is not required to suspend the cells; however, some fluid motion is required for adequate mass transport. A differential rotation mode is used where the inner cylinder and disk rotate together at a higher rate than the outer wall. The disk rotation drives a secondary flow pattern in the radial-axial plane that enhances mixing and mass transport. However, care must be taken to insure that rotation rates are chosen that will provide adequate mass transport and proper cell suspension without clustering cells in one end or centrifuging them to the wall.

NUMERICAL MODEL

The mathematical model and numerical solution method for the flow field are given for completeness. For details of the solution techniques, see Begley (1999).

Mathematical Model

Because of the very limited rotation rates required to maintain low mechanical stress levels, the flow must remain laminar. The fluid is assumed to be incompressible and of uniform density and viscosity. The symmetry of the geometry and boundary conditions leads to the assumption of an axisymmetric flow field. The resulting momentum and continuity equations in cylindrical coordinates are:

$$u\frac{\partial u}{\partial r}-\frac{v^2}{r}+w\frac{\partial u}{\partial z}=\frac{1}{Re}\left[\frac{\partial}{\partial r}\left(\frac{1}{r}\frac{\partial}{\partial r}(ru)\right)+\frac{\partial^2 u}{\partial z^2}\right]-\frac{\partial P}{\partial r}$$

$$u\frac{\partial v}{\partial r}-\frac{uv}{r}+w\frac{\partial v}{\partial z}=\frac{1}{Re}\left[\frac{\partial}{\partial r}\left(\frac{1}{r}\frac{\partial}{\partial r}(rv)\right)+\frac{\partial^2 v}{\partial z^2}\right]$$

$$u\frac{\partial w}{\partial r}+w\frac{\partial w}{\partial z}=\frac{1}{Re}\left[\frac{1}{r}\frac{\partial}{\partial r}\left(r\frac{\partial w}{\partial r}\right)+\frac{\partial^2 w}{\partial z^2}\right]-\frac{\partial P}{\partial z}$$

and

$$\frac{\partial u}{\partial r}+\frac{u}{r}+\frac{\partial w}{\partial z}=0$$

The solution is independent of the azimuthal direction and can be obtained in a radial-axial plane as shown in the upper portion of Figure 2.

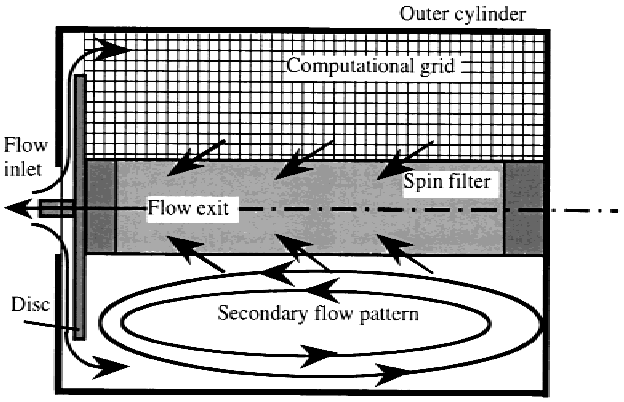

Figure 2. Basic flow pattern and numerical grid for the RWPV.

The flow pattern can be visualized using the intersections of stream surfaces with a radial-axial plane. For the steady-state solution, these lines would coincide with fluid element's paths viewed in a plane rotating in the azimuthal direction with the fluid element. These lines are called streamlines, although they are not tangent to the local velocity vectors (only the radial and axial components). It should always be remembered that the primary fluid motion is in the azimuthal direction.

Mean Shear

Because of the high sensitivity of mammalian cells to mechanical stress levels, it is useful to define a measure of the mechanical shear forces that exist in the flow field. The three shear stress components in the fluid are:

$$S_{r\theta} = \mu\left[r \frac{\partial}{\partial r}\left(\frac{v}{r}\right) \right]$$

$$S_{\theta z} = \mu\left[\frac{\partial v}{\partial z}\right]$$

and

$$S_{rz} = \mu\left[\frac{\partial w}{\partial r} + \frac{\partial u}{\partial z}\right]$$

These act on three mutually perpendicular (coordinate plane) areas to produce the resulting traction forces. Thus, a meaningful metric of the shear force per unit area (Begley, 1999) is:

$$S_m = \frac{1}{3}(S_{r\theta}^2 + S_{\theta z}^2 + S_{rz}^2)^{1/2}$$

This measure will be used to compare the stress levels in the RWPV operated under different operating conditions. It must be remembered that this measure does not include shear forces resulting from relative motions due to density differences existing in acceleration fields. As will be shown in a subsequent report, the shear levels resulting from relative motions are typically much larger than the fluid shear levels. The fluid mean stress levels are useful as a lower limit of shear stress for the cells and for comparing different operating conditions.

Numerical Method

The computational grid for the velocity components is indicated in the upper portion of Figure 2. A radial-axial grid of 44 × 176 nodes was used for the flow field solutions. Because the pressure on the boundaries is not known a priori, a staggered mesh was employed. Because only steady-state solutions are of interest, a pseudo-compressibility method was used with typically 6000 iterations to reach convergence. Grid size, stability, and convergence were investigated prior to obtaining the final solutions.

EXPERIMENTAL VALIDATION

To validate the mathematical model and numerical solution method, experimental measurements were made in a full-scale Plexiglas model of the RWPV. The model was complete with perfusion and was enclosed in a rectangular glass vessel filled with water to minimize optical distortions due to refractive index differences. A single-component Dantec laser Doppler velocimeter (LDV) with a 10-mW He–Ne Laser and an 80-mm focusing lens provided a very small sampling volume. The entire LDV system was mounted on a computer-controlled traversing system with motion in all three coordinate directions. The LDV system used a Bragg cell to allow flow direction determination as well as accurate velocity component determination at the very low velocities encountered in the RWPV. Radial positions were corrected for beam refraction.

The results of the measured azimuthal and axial velocity components are compared with the corresponding numerical predictions in Figure 3. The axial reference position is at the disk surface. Radial plots of the azimuthal and axial components of velocity at the same axial measurement location are shown side by side. The axial locations are indicated on each plot.

The agreement between the measured and computed profiles is very good, with differences generally <5%. For the case shown, this corresponds to an absolute error of about 0.5 mm/s, well within the uncertainty of the measurements.

NUMERICAL FLOW FIELD RESULTS

Flow fields were computed for a range of both microgravity (Begley, 1999) and ground-based operating conditions. Clearly, in the absence of large density gradients in the fluid media, the flow field for a given set of operating conditions will be the same at 1*g* and microgravity. The reason for the difference in operating conditions is that the cell–microcarrier assemblages will not suspend in 1*g* using microgravity operating conditions and, conversely, the solid-

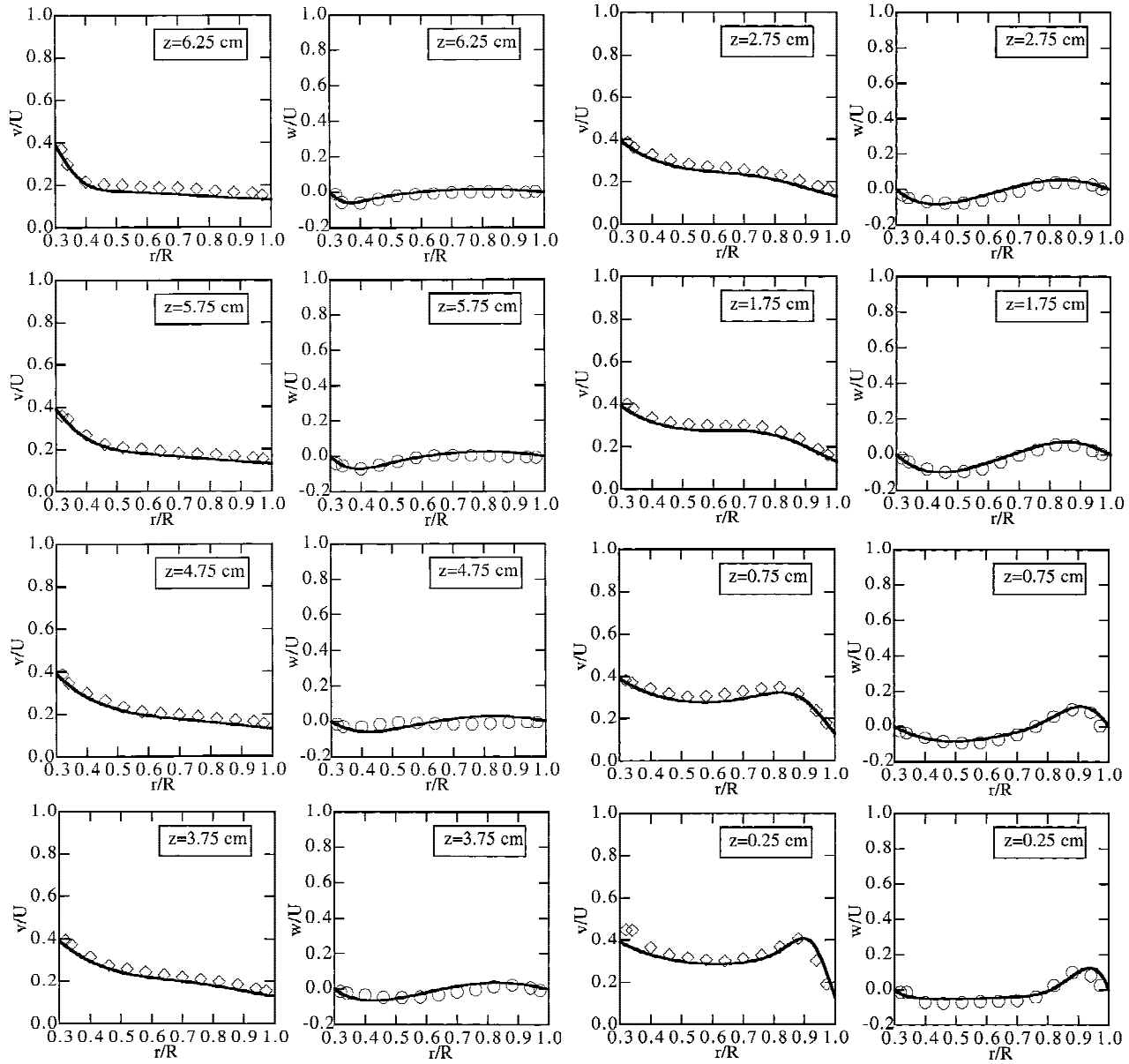

Figure 3. Velocity component comparison with experiment (10-rpm inner, 1-rpm outer rotation, perfusion rates 10 cm^3/min). Solid lines represent numerical simulation predictions, diamonds indicate measured azimuthal velocity, and circles indicate measured axial velocity. Axial locations for each graph are shown.

body rotation mode used for 1*g* would simply centrifuge the cells to the outer wall in microgravity.

To illustrate the effect of operating conditions on the secondary flow, streamlines representing the intersection of stream surfaces with the radial-axial plane are shown in the following figures. The disk (left) and spin filter (bottom) are shown in gray with the perfusion inlet in the gap between the disk and the outer wall (upper left). In each sequence of figures, the vessel centerline is at the bottom of the lowest plot; however, it is not shown in the upper plots to save space. The streamlines are drawn at equal increments in each plot so that flow rate comparisons between various operating conditions can be made visually from the streamline figures. However, for 1*g* operating conditions, the streamlines are consistently drawn with tenfold smaller increments than the microgravity streamlines due to the much weaker secondary flow in the solid-body rotation cases.

Microgravity Conditions

In microgravity, the vessel operates with a low rotation rate for the outer cylinder and a higher rate for the spin filter and disk assembly. A Couette flow situation (without the disk) would result in a flow pattern with at least two counterrotating cells, which would inhibit axial mass transport and increase the possibility of cell-to-cell impacts. With the viscous pump disk in place, the imbalance between the pressure gradient and the centrifugal force near the surface of

the disk produces a significant radial acceleration. Continuity requires that the fluid above the disk travels axially to compensate for the radial flow. The resulting flow field is an elongated circulation pattern with no counterrotation, as shown in Figure 4 for typical microgravity operating conditions.

The effects of increased differential rotation rate (the difference between the inner and outer rotation rates) are also shown in Figure 4. In this figure, the outer wall rotation and the perfusion rates are held constant at 1 rpm and 5 cm^3/min, respectively. The differential rotation rate is increased from top to bottom by increasing the inner rotation rate as follows: 5 rpm (Fig. 4a); 10 rpm (Fig. 4b); and 15 rpm (Fig. 4c). The differential rotation rate strongly increases the strength of the radial-axial flow, which would enhance the distribution of fresh fluid media throughout the vessel.

The effect of perfusion on the radial-axial flow for microgravity operating conditions is shown in Figure 5. In each plot, the operating conditions are 5-rpm inner, 1-rpm outer rotation rates with a typical range of perfusion rates: 1 cm^3/min (Fig. 5a); 5 cm^3/min (Fig. 5b); and 10 cm^3/min (Fig. 5c). Note that the number of streamlines intersecting the spin filter is indicative of the different perfusion rates. For this particular set of operating conditions, a small, corotating cell is evident at the far right end of the vessel that decreases in size and strength with increasing perfusion. Increases in perfusion rate cause a slight increase in the strength of the secondary flow as evidenced by both the shape of the flow pattern and the increased number of streamlines. However, this effect is minimal compared to the dominant effect of the differential rotation rate at these typical operating conditions.

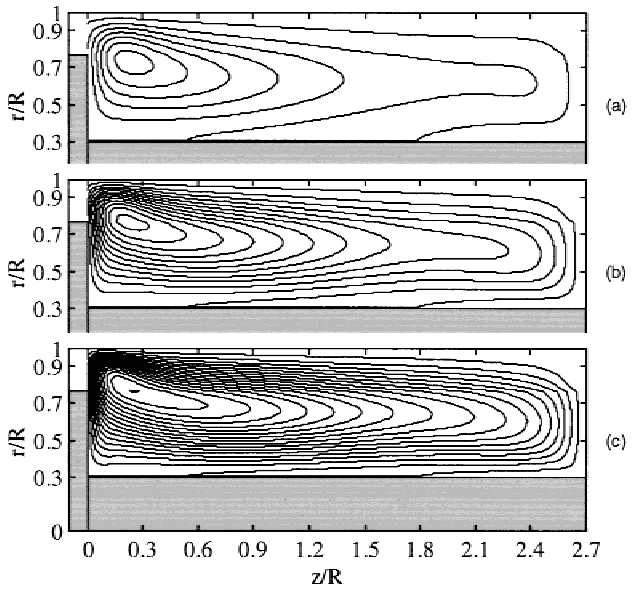

Figure 4. Effect of differential rotation on radial-axial flow, for microgravity operation (1-rpm outer rotation, perfusion rates 10 cm^3/min). Increased circulation for (a) 5-rpm, (b) 10-rpm, and (c) 15-rpm inner rotation rates.

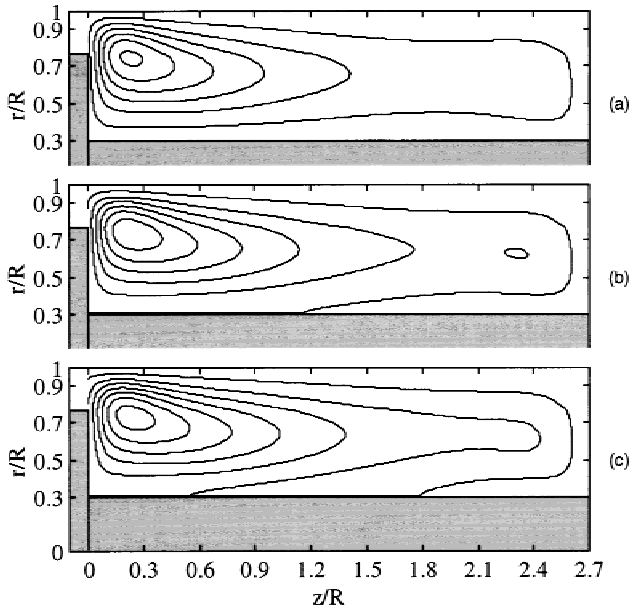

Figure 5. Effect of perfusion on radial-axial flow, for microgravity operation (5-rpm inner, 1-rpm outer rotation rates). No significant effect for perfusion rates of (a) 1 cm^3/min, (b) 5 cm^3/min, and (c) 10 cm^3/min.

Although the differential rotation rates are important for determining the strength of the secondary flow, the mean rotation rate also has an influence on the flow pattern. The importance of outer wall rotation is shown in Figure 6 for varying differential rotation rates of 6 rpm (Fig. 6a) and 11 rpm (Fig. 6b). With no outer wall rotation both cases show flow patterns that break down into three counterrotating cells. Outer wall rotation is required to eliminate this type of flow field instability at these conditions.

Increasing the outer wall rotation rate above the 1-rpm cases shown previously has a tendency to make the flow field more uniform. However, at some point an increased mean rotation will have the effect of centrifuging cells to the outer wall in microgravity.

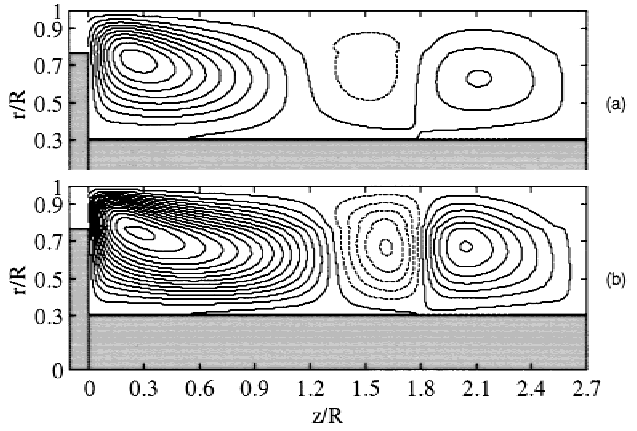

Figure 6. Importance of outer wall rotation for microgravity operation (0-rpm outer wall rotation, perfusion 10 cm^3/min). Three-fluid-cell pattern for inner rotation rates of (a) 6 rpm and (b) 11 rpm.

Ground-Based Conditions

In the 1*g* control experiment and Earth-based "microgravity simulations," the vessel operates with the same rotation rate for both the outer cylinder and the spin filter and disk assembly. Because there is no differential rotation rate, the fluid moves almost as a solid body, while the perfusion rate becomes the primary radial-axial transport mechanism. The radial-axial flow field resulting from the 1*g* solid-body rotation mode is much weaker than even the lowest differential rotation case shown previously in Figure 4a for microgravity conditions. In order to show the 1*g* flow fields, the increment between streamlines has been reduced to one tenth the increment used for the microgravity plots. Figure 7 shows the streamlines for the 15-rpm solid-body rotation mode with varying perfusion rates of 1 cm^3/min (Fig. 7a), 5 cm^3/min (Fig. 7b), and 10 cm^3/min (Fig. 7c).

As the cells grow and form cell-microcarrier aggregates, the solid-body rotation rate must be increased to maintain adequate suspension as the experiment progresses. Figure 8 shows the change in radial-axial flow field as the rotation rate is increased while maintaining a constant perfusion rate of 5 cm^3/min. At the beginning of the cell experiment, the 15-rpm case (Fig. 8a) seems to have a fairly good distribution of inlet fluid; however, six of nine streamlines pass very close to the disk and the opposite cylinder wall and then go directly to the perfusion exit. This indicates that at least 50% of the inlet fluid is transported directly to the exit without passing through the bulk of the vessel volume. As the solid-body rotation rate is increased, this situation worsens until, at the end of the experiment at 35 rpm (Fig. 8c), nearly 80% of the inlet fluid "short circuits" the vessel volume.

This behavior is characteristic of flows in rotating reference frames or nearly solid-body rotation. As the fluid is forced toward the axis of rotation by the perfused fluid, it is accelerated in the azimuthal direction as a consequence of conservation of angular momentum. This slight increase in azimuthal velocity is retarded near the end caps by the viscous no-slip condition at the slower moving walls. This slower moving fluid is accelerated by the imposed pressure gradient, established by the faster fluid outside the viscous region, toward the spin filter. The higher the rotation rate, the stronger the radial pressure gradient and the larger the fraction of fluid accelerated in the viscous boundary layers at the end caps.

The same effect can be explained from vorticity considerations. Figure 9 shows plots of axial vorticity components for the same operating conditions. In a solid body rotation at steady state, all of the fluid has uniform vorticity equal to twice the rotation rate. As fluid is pumped radially inward in the viscous regions of the end caps, the axial vorticity is slightly stretched and intensified as indicated by the increasing values of isovorticity (axial component) contours with decreasing radius. Radial and azimuthal vorticity components are formed in the viscous end cap regions.

MEAN SHEAR RESULTS

The RWPV was designed to produce laminar flow conditions and to provide a lower shear environment for mammalian cell culture compared to traditional bioreactors. For these calculations, we look at the mean shear environment in the fluid without considering the additional shear stress at

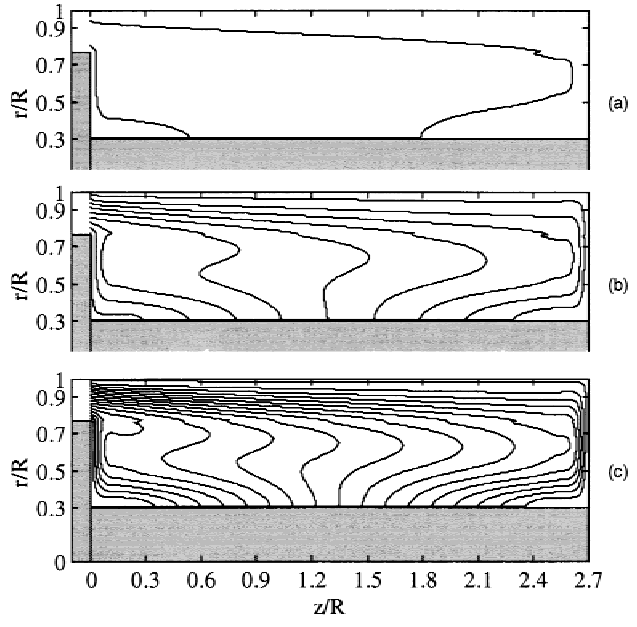

Figure 7. Effect of perfusion on radial-axial flow for ground-based operating conditions (15-rpm inner, 15-rpm outer rotation rates). Increasing flow bypass for perfusion rates of (a) 1 cm^3/min, (b) 5 cm^3/min, and (c) 10 cm^3/min.

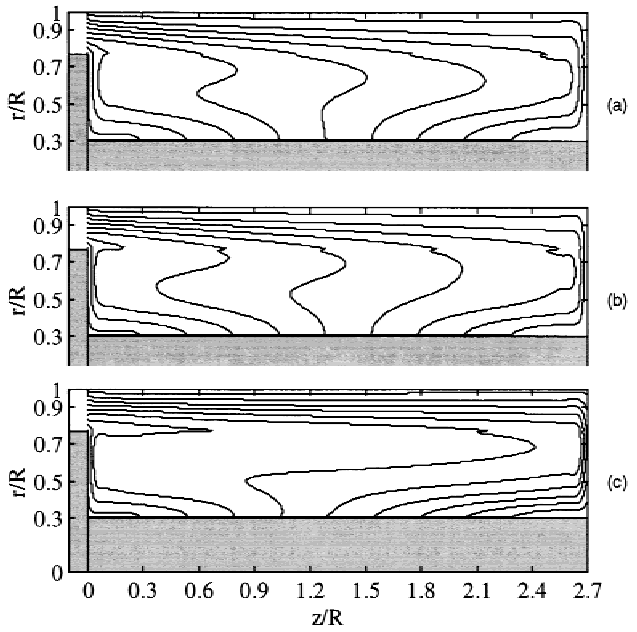

Figure 8. Effect of solid-body rotation rate on radial-axial flow for ground-based operating conditions (perfusion rates 5 cm^3/min). Increasing flow bypass for solid-body rotation rates of (a) 15, (b) 25, and (c) 35 rpm.

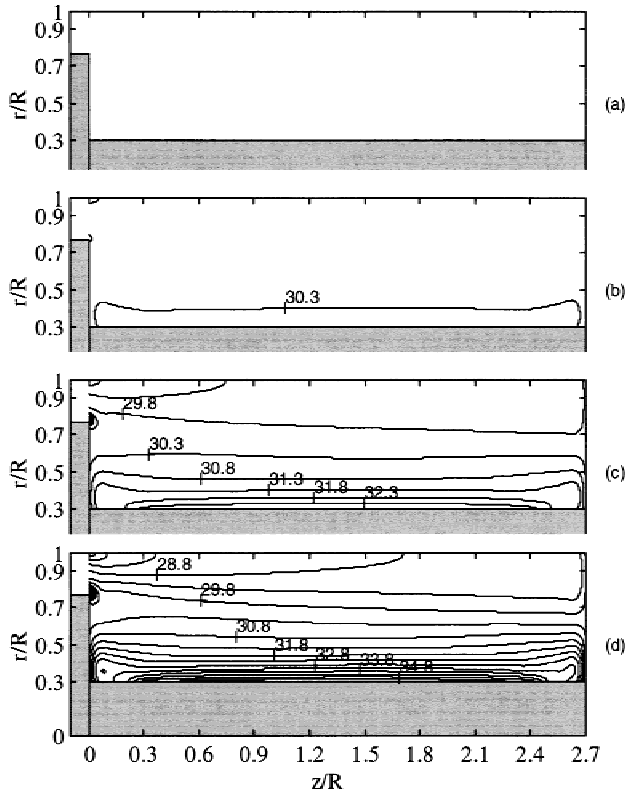

Figure 9. Effect of perfusion on axial vorticity for ground-based operating conditions (15-rpm inner, 15-rpm outer rotation rates). Vorticity nonuniformity increases for perfusion rate of (a) 0 cm^3/min, (b) 1 cm^3/min, (c) 5 cm^3/min, and (d) 10 cm^3/min.

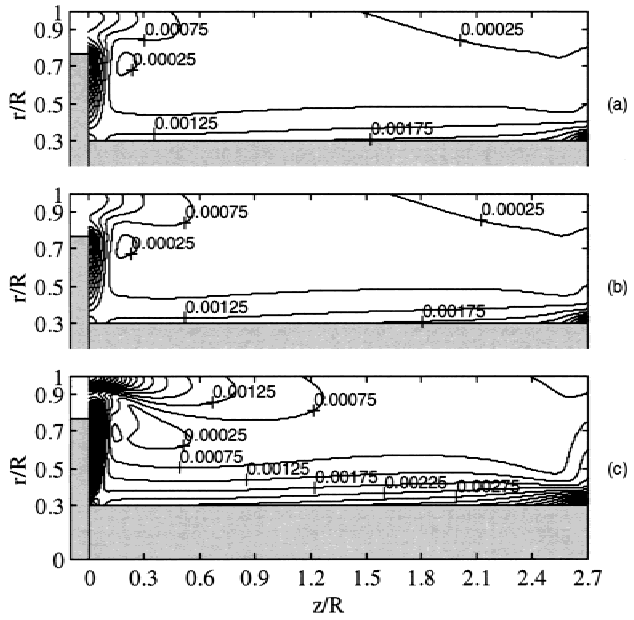

Figure 10. Mean shear comparison for microgravity operating conditions (dyne/cm^2). Small increases with perfusion rate and larger changes with rotation rate: (a) 5-rpm inner, 1-rpm outer rotation, and perfusion rate 5 cm^3/min; (b) 5-rpm inner, 1-rpm outer rotation, and perfusion rate 10 cm^3/min; (c) 10-rpm inner, 1-rpm outer rotation, and perfusion rate 10 cm^3/min.

the cell surface due to the relative movement of the cells within the fluid.

The mean shear stress levels for microgravity conditions are shown in Figure 10. The mean shear stress levels are quite low throughout the majority of the vessel with peak values near the disk and the corner between the spin filter and outer wall. The first two plots compare the effect of increased perfusion rate since they have the same rotation rates, 5-rpm inner, 1-rpm outer, with part (Fig. 10a) at the perfusion rate of 5 cm^3/min and part (Fig. 10b) at 10 cm^3/min. There is very little shear stress increase even when doubling the perfusion rate. The second two plots compare differential rotation rates with the same perfusion rate, 10 cm^3/min, with part (Fig. 10c) at three times the inner rotation rate, 15 rpm. There is a clear increase in shear stress with an increase in differential rotation rate; however, the shear numbers are still small.

The mean shear stress levels for 1*g* operating conditions are quite different. In a true solid body rotation, there should be a completely uniform, zero-shear-stress environment in the vessel. However, for the 1*g* control experiment, the perfusion rate creates a small but fairly uniformly distributed shear environment in the vessel, as shown in Figure 11. The first two plots compare 15-rpm solid-body rotation mode with perfusion rates of 5 cm^3/min (Fig. 11a) and 10 cm^3/min (Fig. 11b). As in the microgravity case, there is only a slight increase in shear stress with increased perfusion rate. However, the effect of increasing the solid-body rotation rate from 15 rpm (Fig. 11b) to 25 rpm (Fig. 11c) nearly doubles the shear levels. Thus, the effect of increased

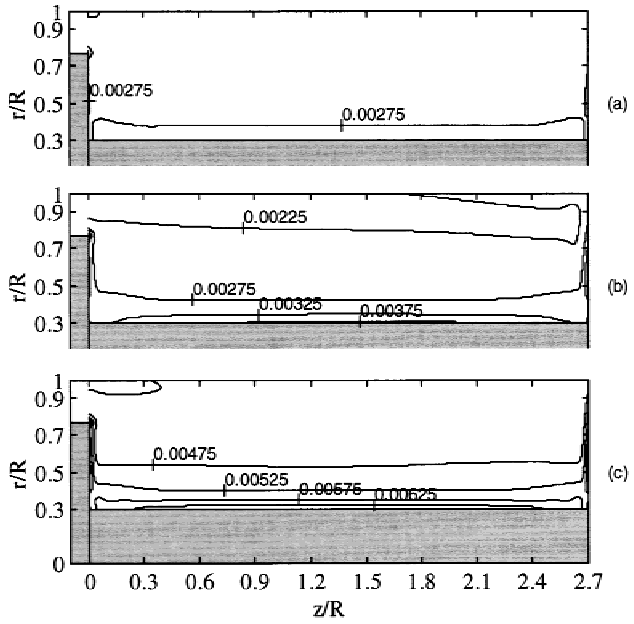

Figure 11. Mean shear comparison for ground-based operating conditions (dyne/cm^2). Small increases with perfusion rate and larger changes with rotation rate (a) 15-rpm inner, 15-rpm outer rotation, and perfusion rates 5 cm^3/min; (b) 15-rpm inner, 15-rpm outer rotation, and perfusion rates 10 cm^3/min; and (c) 25-rpm inner, 25-rpm outer rotation, and perfusion rates 10 cm^3/min.

shear levels is a result of the presence of perfusion, but depends primarily on the rotation rate. Again, the overall shear numbers are still very small.

The mean shear stress histograms in Figure 12 show the percent of the vessel volume that is at varying shear levels for both microgravity and 1*g* operating conditions. In the microgravity cases, the maximum shear calculated (0.0196 dyne/cm^2 for the 5-rpm inner and 0.0437 dyne/cm^2 for the 10-rpm inner case) is higher than the maximum shear of the 1*g* cases (0.0049 dyne/cm^2 for 15 rpm and 0.0082 dyne/cm^2 for 25 rpm). However, these peak shear numbers only represent <1% of the vessel volume. As shown in the histogram, the majority of the vessel volume in the microgravity cases (97% for 5-rpm inner and 88% for 15-rpm inner) is at or below 0.002 dyne/cm^2. The 1*g* solid body cases are higher with 99.9% of the volume in the 15-rpm case at 0.004 dyne/cm^2 and 97% of the volume for the 25-rpm case at 0.006 dyne/cm^2.

DISCUSSION

The shear-stress calculations presented here are based on the flow environment only. Additional shear is experienced by the cell aggregate as it moves through the fluid. In 1*g*, the cells, which are about 4% denser than the fluid media, fall through the fluid at terminal velocity under the influence of gravity. In microgravity, the centripetal acceleration becomes the dominant body force. Using the maximum velocity at the disk tip for the 10-rpm inner, 1-rpm outer case, the centripetal acceleration is on the order of 0.02 m/s^2 compared to the 9.8 m/s^2 acceleration of gravity. For a 2-mm cancer-cell assemblage, the Reynolds number, based on relative velocity and cell diameter, is 86 in 1*g* and 0.19 maximum in microgravity. Based on a uniform flow at these relative velocities, this corresponds to a maximum surface shear stress of 0.002 dyne/cm^2 in microgravity compared to 1.1 dyne/cm^2 in the 1*g* control experiment. Thus, for the ground-based conditions, the effect of the increased fluid shear levels (due to perfusion) with equal rotation rates is insignificant compared with that due to the relative motion. However, in microgravity conditions, the shear levels experienced by the cells on microcarriers depends upon the operating conditions and can be varied from 0.002 dynes/cm^2 to much higher levels depending upon mass transport requirements.

In the 1*g* control experiment, the hydrodynamic boundary layer is thin and the mass transport is primarily determined by the concentration distribution within the vessel. The lower Reynolds number range experienced in microgravity indicates a thick viscous region at the surface of the cell, which could inhibit mass transport due to the longer diffusion times. The Schmidt number for oxygen transport is about 400, and glucose is 1400. In the aforementioned example, this gives a Peclet number for oxygen mass transport of 34,400 in 1*g* and 76 in microgravity. The inverse of the Peclet number can be thought of as an indication of the thickness of the gradient region for mass transport. Using standard correlations, the overall mass transport rate, as indicated by the Sherwood number, for oxygen transport in microgravity is less than two times the diffusion limit, whereas in 1*g* it is 22 times the diffusion limit. This implies that operation of the RWPV in microgravity could easily become mass transport limited, and careful selection of operating conditions is essential.

As shown previously, the flow patterns for the ground-based conditions would suggest that the concentration distributions might be quite nonuniform when utilization or production rates are large. Differential rotation rates (with the inner wall rotating faster) could distribute the perfused flow more uniformly. Details of the mass transport in the RWPV will be presented in a subsequent article.

CONCLUSIONS

1. The numerical flow-field model was validated using LDV measurements, showing agreement within 0.5 mm/s.

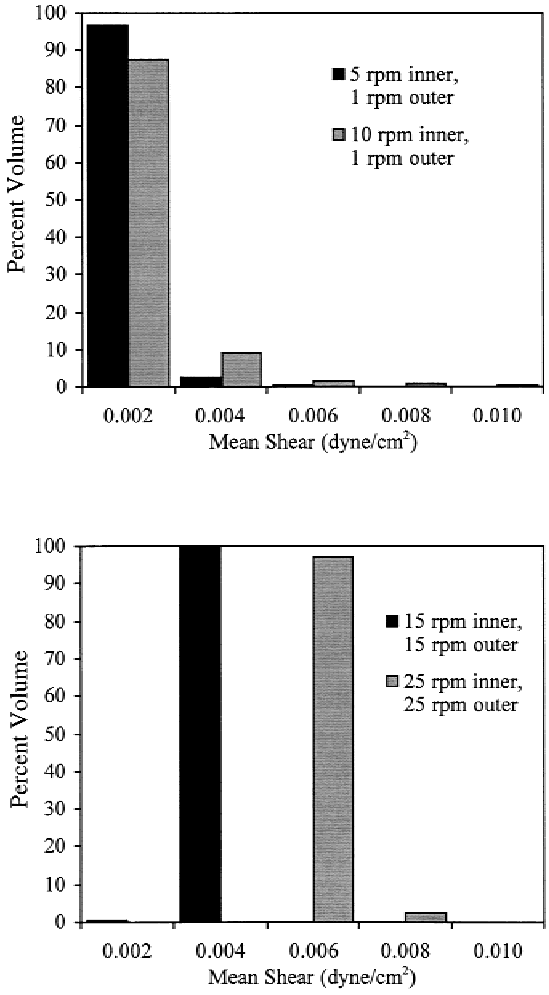

Figure 12. Mean shear histograms. All calculations are for perfusion rates of 10 cm^3/min. Conditions are shown for (a) microgravity and (b) ground-based conditions.

2. Microgravity differential rotation operating conditions produce a significantly different flow environment than ground-based solid-body rotation operating conditions.
3. Increased differential rotation rates strengthen the secondary flow, enhancing the radial-axial distribution of inlet fluid, while maintaining acceptably low mean shear stress levels.
4. Increased solid-body rotation rate adversely affects mass transport as 50% to 80% of the inlet fluid bypasses the bulk of the vessel volume.
5. Changes in perfusion rates, for typical mammalian cell cultures, have little effect on the secondary flow fields and mean shear environments in both microgravity and ground-based operating conditions.
6. The mean shear-stress levels in the fluid in both microgravity and unit gravity are similar in magnitude. The mean shear-stress levels for the ground-based fluid environment are negligible compared to the local shear stresses expected at the cell surface due to the settling velocities in Earth's gravity. The lower relative velocities expected in microgravity could produce cell surface shear levels comparable to the mean shear levels calculated for the fluid environment.

NOMENCLATURE

R	length scale, vessel outer diameter 2.5 cm
Re	Reynolds number based on tip velocity
s_m	mean shear stress
U	velocity scale, largest of disk or outer wall azimuthal velocity
u	radial velocity
v	azimuthal velocity
w	axial velocity
r	radial coordinate
z	axial coordinate
μ	fluid viscosity
μg	microgravity
θ	azimuthal coordinate
$1g$	acceleration of gravity (9.8 m/s^2)

References

Begley CM. 1999. Fluid dynamic studies of the NASA/JSC RWPV bioreactor for cell culture in microgravity. PhD dissertation. Houston, TX: University of Houston.

Cherry RS, Papoutsakis ET. 1986. Hydrodnamic effects on cells in agitated tissue culture reactors. Bioproc Eng 1:29–41.

Freed LE, Langer R, Martin I, Pellis NR, Vunjak-Novakovic G. 1997. Tissue engineering of cartilage in space. Proc Natl Acad Sci 94: 13885–13890.

Goodwin TJ, Jessup JM, Wolf DA. 1992. Morphologic differentation of colon carcinoma cell lines HT-29 and HT-29KM in rotating wall vessels. In Vitro Cell Dev Biol 28A:7–60.

Goodwin TJ, Prewett TL, Wolf DA, Spaulding GF. 1993. Reduced shear stress: a major component in the ability of mammalian tissues to form three-dimensional assemblies in simulated microgravity. J Cell Biochem 51:301–311.

Kleis SJ, Shreck S, Nerem RM. 1990. A viscous pump bioreactor. Biotechnol Bioeng 36:771–777.

van Wezel AL. 1973. Microcarrier cultures of animal cells. In: Kruse PF, Patterson MK, editors. Tissue culture: methods and applications. New York: Academic Press. p 372–377.